



Time-reversal symmetry breaking, collective modes, and Raman spectrum in pair-density-wave states



Yi-Ming Wu¹ ✉, Andrey V. Chubukov², Yuxuan Wang³ & Steven A. Kivelson⁴

Inspired by empirical evidence of the existence of pair-density-wave (PDW) order in certain underdoped cuprates, we investigate the collective modes in systems with unidirectional PDW order with momenta $\pm \mathbf{Q}$ and a d -wave form-factor with special focus on the amplitude (Higgs) modes. In the pure PDW state, there are two overdamped Higgs modes. We show that a phase with co-existing PDW and uniform (d -wave) superconducting (SC) order, PDW/SC, spontaneously breaks time-reversal symmetry—and thus is distinct from a simpler phase, SC/CDW, with coexisting SC and charge-density-wave (CDW) order. The PDW/SC phase exhibits three Higgs modes, one of which is sharply peaked and is predominantly a PDW fluctuation, symmetric between \mathbf{Q} and $-\mathbf{Q}$, whose damping rate is strongly reduced by SC. This sharp mode should be visible in Raman experiments.

A pair density wave (PDW) is an exotic form of superconducting order in which Cooper pairs carry finite center-of-mass momentum^{1–19}. Many recent experiments have reported possible signatures of PDW order in the absence of a magnetic field in correlated electronic systems, such as kagome metals^{20–26}, NbSe₂^{27–29}, UTe₂^{30–32}, EuRbFe₄As₄³³, SrTa₂S₅³⁴ and rhombohedral graphene³⁵. Certain La-based underdoped high T_c cuprates, such as La_{2– x} Ba _{x} CuO₄ (LBCO) and La_{2– x} X _{y} Sr _{x} CuO₄ with X=Nd (LNSCO) or X=Eu (LESCO) are the most intensely studied PDW candidate materials, where the bulk superconducting (SC) T_c has a deep minimum at $x \approx 1/8$, while the ordering temperature for a stripe charge-density wave (CDW), T_{cdw} , is maximal³⁶. At $T_c < T < T_{cdw}$ transport measurements suggest a dynamical decoupling of the Cu-O layers^{37–47}, which is plausibly explained by the existence of in-plane stripe PDW order with twice the period of the CDW. Below T_c , this PDW order most plausibly coexists with a d -wave SC order⁴⁸.

However, obtaining *direct* experimental evidence of PDW order has proven difficult. Transport properties can be difficult to interpret uniquely in complex materials. STM is another commonly used technique to provide evidence of PDW order^{49–51}. However, STM measurements provide information about surface states, and evidence of order can be difficult to disentangle from signatures of quasiparticle interference⁵². More fundamentally, it is unclear to what extent STM can distinguish a PDW state from a CDW+SC state. Given that a PDW is a “new phase of matter,” more direct and unambiguous experimental signatures are needed. An important experimental development in this direction is a recent X-ray study of underdoped LBCO and La_{2– x} Sr _{x} Cu_{1– y} Fe _{y} O₄⁵³ that apparently provides

bulk evidence for the coexistence of PDW and uniform SC order in a range of T .

In this paper, we study low energy amplitude and phase collective modes in a system of unidirectional d -wave PDW order^{54–56} with and without coexisting d -wave SC order. In the pure PDW state we find the amplitude (Higgs) modes are overdamped. In the PDW+SC state, we find that (i) the system favors spontaneous time-reversal symmetry breaking (TRSB) and (ii) one of the amplitude (Higgs) modes is nearly delta-function-like. Such a sharp mode is predominantly from the synchronous motion of the two PDW amplitude modes with \mathbf{Q} and $-\mathbf{Q}$, and its damping is almost completely eliminated by the presence of uniform SC order. This mode should be visible in non-resonant Raman scattering measurements^{57–67}, which then can be used as a versatile tool in the search for bulk evidence of PDW order. For comparison we also consider a coexisting CDW and SC state, which has been frequently discussed for La-based cuprates, see e.g.^{44,68–73}. We argue that Raman experiments can distinguish between CDW +SC and PDW + SC states, at least when SC order is larger than the order with which it coexists.

Results

Free energy at mean-field level

To enable explicit calculations, we consider a specific microscopic model of PDW order on a square lattice designed to represent one Cu-O layer. The fermion dispersion is taken to be $\xi(\mathbf{k}) = -2t [\cos k_x + \cos k_y]$

¹Stanford Institute for Theoretical Physics, Stanford University, Stanford, CA, 94305, USA. ²Department of Physics, University of Minnesota, Minneapolis, MN, 55455, USA. ³Department of Physics, University of Florida, Gainesville, FL, 32611, USA. ⁴Department of Physics, Stanford University, Stanford, CA, 94305, USA.

✉ e-mail: yimwu@stanford.edu

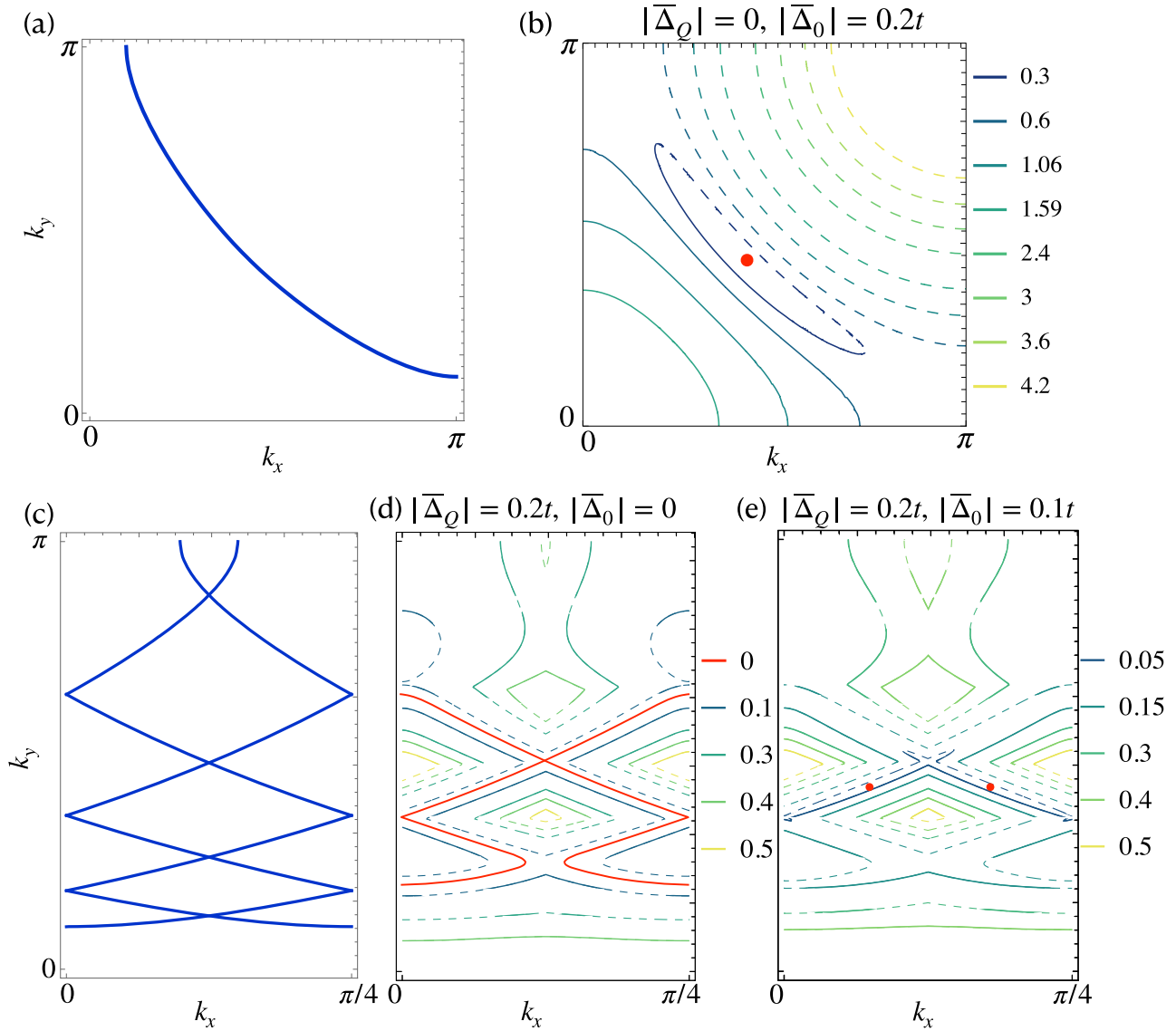


Fig. 1 | Fermi surface (FS) in the original Brillouin zone (BZ). **a** FS without superconducting orders. **b** CEC for a *d*-wave SC in the original BZ for $|\bar{\Delta}_0| = 0.2t$. The red dot indicates the nodal point. The dashed and solid curves are for electron-like and hole-like dispersions, respectively. **c** FS in the folded BZ. **d** CEC for a pure PDW with momentum $\mathbf{Q} = (\frac{\pi}{4}, 0)$ in the folded BZ for $|\bar{\Delta}_{\pm\mathbf{Q}}| = 0.2t$. The red curves indicate the residual Fermi surfaces. **e** CEC for a PDW+SC case with $\varphi_{\mathbf{Q}} = \varphi_{-\mathbf{Q}}$ and $\varphi_0 = \pi/2 + \varphi_{\mathbf{Q}}$ and with $|\bar{\Delta}_0| = 0.1t$ and $|\bar{\Delta}_{\pm\mathbf{Q}}| = 0.2t$. Different colors correspond to different energies, specified to the right of each panel.

$-4t' \cos k_x \cos k_y - \mu$. We choose $t' = -t/4$ and report all energies in units of t . The chemical potential μ is chosen to set $x = 1/8$, resulting in the Fermi surface in Fig. 1a. The PDW and SC order parameters $\Delta(\mathbf{R}, \tau; \mathbf{r})$ are taken to be of the form

$$\Delta(\mathbf{R}, \tau; \mathbf{r}) = \sum_{\bar{\mathbf{q}}=0, \pm\mathbf{Q}} \Delta_{\bar{\mathbf{q}}}(\mathbf{R}, \tau) e^{i\bar{\mathbf{q}}\cdot\mathbf{R}} f(\mathbf{r}) \quad (1)$$

where τ is an imaginary time, $\bar{\mathbf{q}} = 0$ for the uniform SC order and $\bar{\mathbf{q}} = \pm\mathbf{Q}$ for the two PDW orders^{74–76}, and \mathbf{R} and \mathbf{r} denote the center-of-mass and relative positions of the two fermions in a Cooper pair. The Fourier transform of $f(\mathbf{r})$ is the pairing form factor, which we take to have the $d_{x^2-y^2}$ form, $f_{\mathbf{k}} = \cos k_x - \cos k_y$. We assume a period-8 PDW order so $\mathbf{Q} = (\frac{\pi}{4}, 0)$.

At the mean field level, $\Delta_{\bar{\mathbf{q}}}(\mathbf{R}, \tau) = \bar{\Delta}_{\bar{\mathbf{q}}} = |\bar{\Delta}_{\bar{\mathbf{q}}}| e^{i\varphi_{\bar{\mathbf{q}}}}$ does not depend on \mathbf{R} and τ . The phase factors $\varphi_{\bar{\mathbf{q}}}$ have to be determined by minimizing the variational free energy. A conventional coupling of these mean field order parameters to band fermions ($\Delta\psi^\dagger\psi^\dagger + h.c$) yields a set of Bogoliubov quasiparticle bands⁷⁷. In Fig. 1b we show the constant energy

contours (CEC) of the first Bogoliubov band above the Fermi level for a pure *d*-wave SC order. In Fig. 1c we show the FS in the folded BZ, and in Fig. 1d, e we show CEC for the PDW states. For a pure PDW order, there are multiple “Bogoliubov Fermi surfaces”^{39,42,78–81}, as shown in Fig. 1d. These Fermi surfaces are further gapped if a uniform SC is also present, see Fig. 1e.

We obtain the effective Ginzburg-Landau (GL) action in terms of $\Delta_{\bar{\mathbf{q}}}(\mathbf{R}, \tau)$ by Hubbard-Stratonovich transformation of the underlying model with 4-fermion interactions (see ref. 77) we obtain

$$\begin{aligned} \mathcal{F}_{\text{MF}} = & \alpha_1 (|\bar{\Delta}_{\mathbf{Q}}|^2 + |\bar{\Delta}_{-\mathbf{Q}}|^2) + \alpha_2 |\bar{\Delta}_0|^2 \\ & + \beta_1 (|\bar{\Delta}_{\mathbf{Q}}|^4 + |\bar{\Delta}_{-\mathbf{Q}}|^4) + \beta_2 |\bar{\Delta}_0|^4 \\ & + \beta_3 |\bar{\Delta}_{\mathbf{Q}}|^2 |\bar{\Delta}_{-\mathbf{Q}}|^2 + \beta_4 |\bar{\Delta}_0|^2 (|\bar{\Delta}_{\mathbf{Q}}|^2 + |\bar{\Delta}_{-\mathbf{Q}}|^2) \\ & + \beta_5 (\bar{\Delta}_0^* \bar{\Delta}_{-\mathbf{Q}}^* \bar{\Delta}_{\mathbf{Q}}^* + c.c.) + \dots \end{aligned} \quad (2)$$

where all the coefficients are convolutions of fermionic propagators with the dispersion set by our microscopic model⁷⁷. In particular, all β_i turn out to be

positive, at least at $T \ll |\bar{\Delta}_Q|, |\bar{\Delta}_0|$. In this situation, \mathcal{F}_{MF} is minimized when $|\bar{\Delta}_Q| = |\bar{\Delta}_{-Q}|$. The relation between the phases of SC and PDW orders is determined by $\beta_5 > 0$, so

$$\varphi_0 - \frac{\varphi_Q + \varphi_{-Q}}{2} = \frac{\pi}{2} + n\pi \quad (3)$$

where n is an integer. Since $\varphi_0 \rightarrow -\varphi_0$ and $\varphi_{\pm Q} \rightarrow -\varphi_{\mp Q}$ under time reversal¹⁸, Eq. (3) is not time-reversal invariant. This implies that in a mixed PDW + SC state the system favors spontaneous TRSB (TRSB in the mixed state does not depend on the phase difference $\varphi_Q - \varphi_{-Q}$, which is arbitrary to the order described by Eq. (2). This phase is fixed once we include the 8th order contribution to \mathcal{F}_{MF} : $-v[(\bar{\Delta}_Q \bar{\Delta}_{-Q}^*)^4 + c.c.]$, which is allowed for the commensurate, period 8 case we have treated. We have computed the prefactor v and found it is positive. Thus, $\varphi_Q - \varphi_{-Q} = m\pi/2$, where m is integer, of which some experimental signatures have been reported in LBCO^{82,83}.

Collective modes

We now go beyond mean-field and consider small fluctuations, which in momentum space we parameterize as^{54,74,84-91}

$$\Delta_{\bar{q}}(q) \approx \bar{\Delta}_{\bar{q}} \left[1 + \mathcal{A}_{\bar{q}}(q) + i\theta_{\bar{q}}(q) \right] \quad (4)$$

where $q = (\omega_m, \mathbf{Q})$ and $\mathcal{A}_{\bar{q}}(q)$ and $\theta_{\bar{q}}(q)$ are the amplitude and phase variations, respectively. They satisfy $\mathcal{A}_{\bar{q}}(-q) = \mathcal{A}_{\bar{q}}^*(q)$, $\theta_{\bar{q}}(-q) = \theta_{\bar{q}}^*(q)$ and $\mathcal{A}_{\bar{q}}(0) = \theta_{\bar{q}}(0) = 0$. It is convenient to introduce a vector basis $\zeta(q) = [\mathcal{A}_Q(q), \mathcal{A}_{-Q}(q), \mathcal{A}_0(q), \theta_Q(q), \theta_{-Q}(q), \theta_0(q)]^T$. Using this basis and truncating the fluctuating part of the GL action S_{GL} at the Gaussian level, we obtain (see⁷⁷ for details)

$$S_{GL}^{(2)} = \sum_q \zeta^T(q) \hat{\Gamma}^{-1}(q) \zeta(-q) \quad (5)$$

The matrix $\hat{\Gamma}^{-1}(q)$ can be thought of as the inverse matrix Green's function for the fluctuating fields (see⁷⁷ for details). The dispersions of the collective modes along the imaginary Matsubara frequency axis $i\omega_n$ can be found by solving for $\det \hat{\Gamma}^{-1}(q) = 0$. To obtain the dispersions along the real frequency axis ω and the spectral functions $B_j(\mathbf{q}, \omega)$ (j labels the collective modes), we use Padé approximants⁹² to implement the analytic continuation $i\omega_n \rightarrow \omega + 0^+$. Here $B_j(\mathbf{q}, \omega) = \frac{-1}{\pi} \text{Im} D_j(\mathbf{q}, \omega)$ and $D_j(\mathbf{q}, \omega)$ is the j -th eigenvalue of $\hat{\Gamma}(q, \omega)$. We will be interested in the spectral functions of the amplitude modes in the long-wavelength limit, and define $B_j(\omega) \equiv B_j(\mathbf{q} = 0, \omega)$. The calculations are done at $T = 0.005t$, which is in all cases that we studied is well below the values of $|\bar{\Delta}_Q|, |\bar{\Delta}_0|$.

Pure PDW and pure SC

When only $\bar{\Delta}_{\pm Q}$ are present, we find two phase and two amplitude collective modes

$$\theta_{\pm}(q) = \frac{\theta_Q(q) \pm \theta_{-Q}(q)}{\sqrt{2}}, \quad \mathcal{A}_{\pm}(q) = \frac{\mathcal{A}_Q(q) \pm \mathcal{A}_{-Q}(q)}{\sqrt{2}}. \quad (6)$$

In Fig. 2a we plot the spectral functions $B(\omega)$ for the two amplitude modes. We see that both modes are strongly overdamped, and the damping is stronger for the \mathcal{A}_+ mode. The fact that $B(\omega)$ for the \mathcal{A}_+ mode peaks at a higher energy than that for the \mathcal{A}_- mode can be understood analytically within the GL action^{54,77}. For comparison we also present $B(\omega)$ for \mathcal{A}_0 when only a d -wave SC is present (yellow curve). Unlike in an s -wave SC, where $B(\omega) \propto 1/\sqrt{\omega^2 - 4|\Delta_0|^2}$, here for a d -wave SC there is no singularity because of nodal quasiparticles, and the broad maximum is at $\omega/|\bar{\Delta}_0| \sim 6$.

PDW with SC

When both Δ_0 and $\Delta_{\pm Q}$ are present, we find three phase and three amplitude eigen modes

$$\begin{aligned} \theta_{+, \pm}(q) &\propto \frac{\theta_Q(q) \pm \theta_{-Q}(q)}{\sqrt{2}} \pm [C_{\theta}(q)]^{\pm 1} \theta_0(q), \\ \theta_{-}(q) &\propto \theta_Q(q) - \theta_{-Q}(q), \\ \mathcal{A}_{+, \pm}(q) &\propto \frac{\mathcal{A}_Q(q) \pm \mathcal{A}_{-Q}(q)}{\sqrt{2}} \pm [C_{\mathcal{A}}(q)]^{\pm 1} \mathcal{A}_0(q), \\ \mathcal{A}_{-}(q) &\propto \mathcal{A}_Q(q) - \mathcal{A}_{-Q}(q), \end{aligned} \quad (7)$$

where $C_{\theta}(q)$ and $C_{\mathcal{A}}(q)$ are two dimensionless numbers. It can be shown that $C_{\theta}(0) = 1/\sqrt{2}$, while $C_{\mathcal{A}}(0)$ depends sensitively on the relative gap magnitudes. We see from Eq. (7) that \mathcal{A}_- is decoupled from \mathcal{A}_0 , although its propagator is affected by the presence of the SC order. For small q , we find $C_{\mathcal{A}} \gg 1$ for $|\bar{\Delta}_0| \gg |\bar{\Delta}_Q|$, and $C_{\mathcal{A}} \ll 1$ for $|\bar{\Delta}_0| \ll |\bar{\Delta}_Q|$. Moreover, when $C_{\mathcal{A}} \gg 1$, we have $\mathcal{A}_{+,+} \approx \mathcal{A}_0$ and $\mathcal{A}_{+,-} \approx \mathcal{A}_+$ [cf. Eq. (6)]; while in the other limit when $C_{\mathcal{A}} \ll 1$, we have $\mathcal{A}_{+,+} \approx \mathcal{A}_+$ and $\mathcal{A}_{+,-} \approx \mathcal{A}_0$ instead. We show our numerical results of $B(\omega)$ for the three amplitude modes in Fig. 2b and c for $|\bar{\Delta}_0| > |\bar{\Delta}_Q|$, $C_{\mathcal{A}} \gg 1$ and $|\bar{\Delta}_0| < |\bar{\Delta}_Q|$, $C_{\mathcal{A}} \ll 1$, respectively. We note for both cases there exist an almost undamped peak for the lowest energy mode, which is predominantly \mathcal{A}_+ .

A sharp Higgs peak is absent in the pure PDW and pure SC cases and thus appears to be a unique feature of mixed PDW+SC order. From an analytic perspective, the case of $|\bar{\Delta}_0| \gg |\bar{\Delta}_Q|$, $C_{\mathcal{A}} \gg 1$ is relatively easy to understand when $|\bar{\Delta}_Q|$ is treated perturbatively. To locate the modes, one has to (i) re-evaluate the frequencies of \mathcal{A}_+ and \mathcal{A}_- from Eq. (6) in the presence of SC within GL action, (ii) include mode-mode coupling between \mathcal{A}_+ and \mathcal{A}_0 so that the eigen modes become $\mathcal{A}_{+, \pm}$ and (iii) re-evaluate the damping rates in the presence of SC. We show the calculations in⁷⁷ and here list the results: On (i), the resulting \mathcal{A}_+ mode frequency remains comparable to $2|\bar{\Delta}_Q|$, as in a pure PDW state, while the frequency of the \mathcal{A}_- mode increases in the presence of stronger SC and becomes comparable to $|\bar{\Delta}_0|$. This is consistent with Fig. 2(b), which shows that the peak in the \mathcal{A}_- mode is at a frequency set by $|\bar{\Delta}_0|$ rather than by $|\bar{\Delta}_Q|$. We note in passing that this effect is caused by the same β_5 term in (2) that is responsible for TRSB. On (ii), mode-mode coupling (level repulsion) shifts the frequency of the \mathcal{A}_{+-} mode to a smaller frequency, comparable to $|\bar{\Delta}_Q|$. On (iii), the \mathcal{A}_- mode is peaked above $2|\bar{\Delta}_0|$ and its damping is not reduced compared to a pure PDW, but the damping rate of the \mathcal{A}_{+-} mode, peaked well below $2|\bar{\Delta}_0|$, is strongly reduced by SC and also by the fact that even in a pure PDW state the damping is very small at $\omega \sim |\bar{\Delta}_Q|$. As a consequence, the \mathcal{A}_{+-} mode becomes almost completely propagating and the corresponding $B(\omega)$ displays a near- δ -function peak (There is a certain similarity between our case and Morr-Pines scenario for the resonance peak in the cuprates⁹³. We also note that the Higgs mode can, in principle, also decay into two quasiparticles of the phase mode θ_- ^{54,94}. This is a higher-order process, not included in our analysis).

Numerical results⁷⁷ for a generic ratio of $|\bar{\Delta}_0|/|\bar{\Delta}_Q|$ and in particular, for the opposite limit $|\bar{\Delta}_0| \ll |\bar{\Delta}_Q|$ as shown in Fig. 2c again show a sharp spectral peak for the lowest energy amplitude mode (note for $C_{\mathcal{A}} \ll 1$ as in Fig. 2c this undamped mode is $\mathcal{A}_{+,+}$). To understand this analytically one needs to go beyond mode-mode coupling analysis (see ref. 77) since even an infinitesimal SC order parameter gaps out the entire Fermi surface (except for the nodal points) thus changing the susceptibilities in a non-perturbative way.

CDW with SC

We now discuss the case of uniform SC coexisting with CDW order. To permit a direct comparison to the PDW +SC state, we take the CDW ordering vector to be $\mathbf{P} = 2\mathbf{Q}$. We also assume the CDW has an electronic origin^{80,61,95,96}, and neglect the presence of optical phonon modes (for comparison, see refs. 97–102). Thus, we parametrize the CDW fluctuations

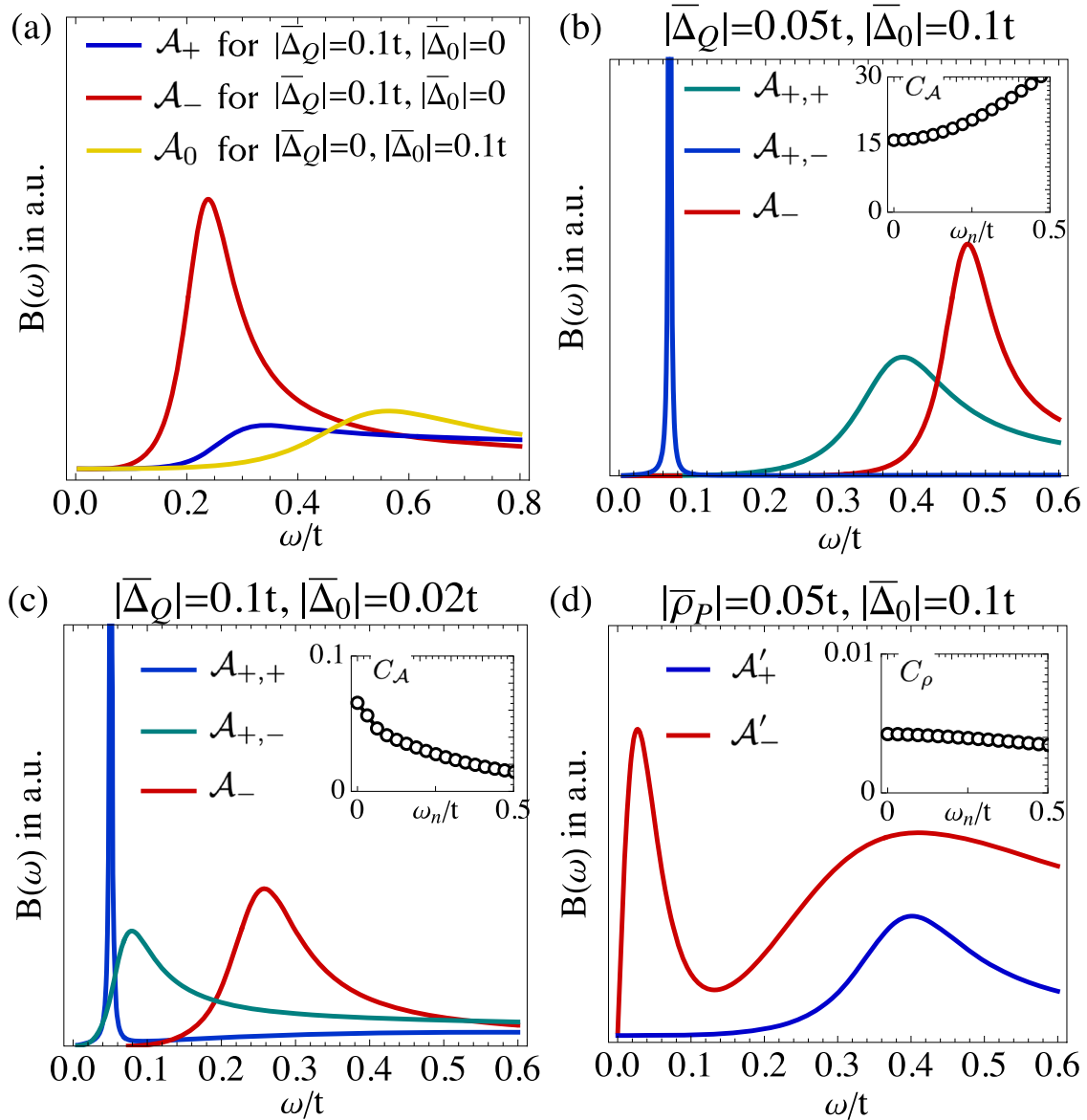


Fig. 2 | Spectral weights of the amplitude modes in various cases. **a** Spectral functions $B(\omega)$ of \mathcal{A}_\pm for a pure PDW order and \mathcal{A}_0 for a pure SC order, both with d -wave form factor. **b** $B(\omega)$ for the three amplitude modes in Eq. (7). The inset shows

C_A as a function of Matsubara frequency ω_n at $\mathbf{q}=0$. In this case $C_A \gg 1$. **c** is similar to **(b)** but with parameters such that $C_A \ll 1$. **d** $B(\omega)$ for the two amplitude modes for the CDW+SC order. The numerical calculations are done at $T = 0.005t$.

as

$$\rho(\mathbf{q}) = 2|\bar{\rho}_p|(1 + \mathcal{A}_p(q)) \cos(\mathbf{P} \cdot \mathbf{r} + \theta_p(q)), \quad (8)$$

where \mathcal{A}_p and θ_p are the CDW amplitude and phase modes (amplitudon and phason). As before, we introduce the attractive interactions in the CDW and SC channels and obtain an effective action for CDW and SC orders. At the mean-field level, we find that the phase of a SC order parameter can be arbitrary, i.e., TRS is not broken. *Importantly, this means that the phase with coexisting SC and PDW order is thermodynamically distinct from the phase with coexisting CDW and SC order!* The part of the action describing fluctuations around mean-field is formally the same as Eq. (5) in a new basis $\zeta' = [\mathcal{A}_p(q), \mathcal{A}_0(q), \theta_p(q), \theta_0(q)]^T$. There are two phase and two amplitude eigenmodes

$$\theta_p(q), \theta_0(q), \mathcal{A}'_\pm \propto \mathcal{A}_0 \pm [C_\rho(q)]^{\pm 1} \mathcal{A}_p. \quad (9)$$

In Fig. 2d we show the spectral functions for the two amplitude modes \mathcal{A}'_\pm . First we note $C_\rho \ll 1$ for the chosen parameters. In fact, C_ρ remains small

even with larger $|\bar{\rho}_p|$ or $|\bar{\Delta}_0|$, meaning $\mathcal{A}'_+ \approx \mathcal{A}_0$ and $\mathcal{A}'_- \approx \mathcal{A}_p$. As in the PDW + SC case, the mode, for which $B(\omega)$ displays a visible peak, largely describes fluctuations of a non-SC order (here, CDW). We see, however, that the peak is substantially broader than in the PDW+SC case.

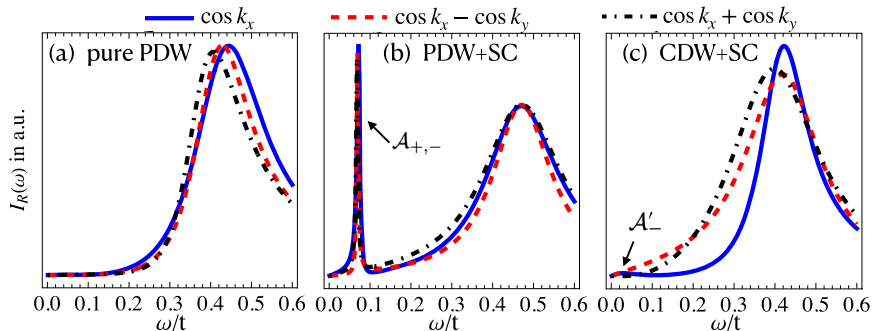
Raman spectrum

We next check whether the sharp mode for the PDW+SC case and a more broadened \mathcal{A}'_- mode for the CDW+SC case can be detected in Raman scattering. For this, we compute dressed Raman susceptibilities defined as $\chi_R(\omega_n) = \int d\tau e^{i\omega_n\tau} \lim_{\mathbf{q} \rightarrow 0} \langle \mathcal{T}_\tau \tilde{\rho}(\mathbf{q}, \tau) \tilde{\rho}(-\mathbf{q}, 0) \rangle$ where \mathcal{T}_τ is the time ordering and $\tilde{\rho}(\mathbf{q}, \tau) = \sum_{\mathbf{k}, \sigma} \gamma(\mathbf{k}) \psi_\sigma^\dagger(\mathbf{k} + \mathbf{q}/2, \tau) \psi_\sigma(\mathbf{k} - \mathbf{q}/2, \tau)$ is the Raman density with the Raman vertex $\gamma_{\mathbf{k}}$. Applying linear response theory^{77,103–108}, we obtain

$$\chi_R(\omega_n) = K(\omega_n) - \Lambda^T(-\omega_n) \hat{\Gamma}(\omega_n) \Lambda(\omega_n). \quad (10)$$

Here $K = \chi_{\bar{\rho}, \bar{\rho}}$ is the bare Raman susceptibility, $\Lambda = \chi_{\zeta, \bar{\rho}}$ is the coupling between the Raman density and a collective mode and $\hat{\Gamma}$ is the susceptibility of the collective mode.

Fig. 3 | Raman intensities in the A-channel with $\gamma(\mathbf{k}) = \cos k_x$ and $\cos k_x \pm \cos k_y$. The parameters are the same as those in Fig. 2(a), (b) and (d) respectively. Collective modes, which chiefly contribute to the peaks in $I_R(\omega)$ are marked.



In the presence of either PDW or CDW order, the original four-fold rotational symmetry of a square lattice is broken down to two-fold, in which case the symmetry group for rotations in the XY plane becomes D_2 . Out of four one-dimensional representations of D_2 , the most relevant ones are $A : \cos k_x, \cos k_y, \cos k_x \pm \cos k_y$ and $B = \sin k_x \sin k_y$ ¹⁰⁵. We consider Raman vertices $\gamma(k)$ with either A or B symmetry. For pure stripe PDW order in either x or y direction, the B_1 Raman channel is inactive, and in the A channel only modes that are even under $\mathbf{Q} \rightarrow -\mathbf{Q}$ are visible. For the PDW+SC case, we find by directly computing χ_R that the \mathcal{A}_{++} and \mathcal{A}_{+-} modes are Raman active, while the \mathcal{A}_- mode is Raman inactive. For the CDW+SC case, \mathcal{A}'_{\pm} are both Raman active.

In Fig. 3 we show the calculated Raman intensity $I_R(\omega) = \frac{-1}{\pi} \text{Im} \chi_R(i\omega_n \rightarrow \omega + i0^+)$, in the A channel with $\gamma(k) = \cos k_x$ and $\cos k_x \pm \cos k_y$, for PDW, PDW +SC, and CDW +SC orders. We see that the Raman intensity is qualitatively the same for all $\gamma(k)$. For a pure PDW [panel (a)], the Raman response is featureless at small frequencies because the \mathcal{A}_- mode, which could potentially give rise to a peak in $I_R(\omega)$ ⁵⁴, is Raman inactive. For PDW+SC order [panel (b)], $I_R(\omega)$ reproduces the sharp peak in the spectral function of the \mathcal{A}_{+-} mode. For the CDW + SC state, $I_R(\omega)$ calculated with $\gamma(k) = \cos k_x$ reproduces a small hump corresponding to \mathcal{A}'_- mode, but this feature is not observed when calculated using $\gamma(k) = \cos k_x \pm \cos k_y$. Based on these results, we argue that Raman scattering can distinguish different ordered states.

Effects of weak disorder

In the presence of weak disorder, the existence of 2D long-range CDW or PDW order is precluded (for incommensurate order this is true even in 3D), and we expect that PDW and CDW order only exists with finite (possibly large) correlation length. The nature of the remaining (vestigial) orders when a pure PDW state is disrupted by weak disorder is not entirely clear^{109,110}. However, a PDW+SC state remains distinct from a CDW+SC state since the TRSB characteristic of the PDW+SC phase should survive as vestigial order for a finite range of disorder strengths.

Another feature of disorder is that it induces a new form of coupling between the uniform SC and PDW orders when they coexist. Such a coupling is realized by a possible 1Q CDW order

$$\rho_{\pm Q}(\mathbf{r}) \sim \left[\Delta_0^*(\mathbf{r}) \Delta_{\pm Q}(\mathbf{r}) + \Delta_{\mp Q}^*(\mathbf{r}) \Delta_0(\mathbf{r}) \right]. \tag{11}$$

In the absence of disorder, TRSB implies that this 1Q order vanishes. However, in the presence of a disorder $V(\mathbf{r})$, there is an additive contribution to the effective action of the form $\mathcal{F}_{dis} = V(\mathbf{r}) \left[\rho_Q(\mathbf{r}) e^{iQ \cdot \mathbf{r}} + c.c. \right]$. Including this contribution in the PDW+SC case and assuming $V(\mathbf{r})$ is short-range correlated we find⁷⁷: 1) At least to lowest order in the disorder strength, the disorder coupling always favors spontaneous TRSB, enforcing the tendency already derived in the clean limit (The physics behind this is the same as that which underlies the disorder driven breaking of TRS in junctions in which the leading order Josephson coupling is frustrated^{111,112}); 2) It induces local

1Q CDW order which is weak (small amplitude) but can have a relatively long correlation length that diverges when $\bar{V}^2 \rightarrow 0$. This sort of disorder-stabilized density-wave correlations is reminiscent of Zn doping stabilized spin-stripe order in LSCO¹¹³ and YBCO¹¹⁴.

It is also important to mention that in materials which exhibit signatures of the coexistence of uniform SC and PDW or uniform SC and CDW orders, it is always questionable whether they coexist uniformly, or if instead they occur in distinct mesoscopic regions of the material, and only truly coexist at the interfaces between regions⁴⁸. Such coexistence could exhibit features quite different from anything we have analyzed.

Discussion

We have found that there is a clear distinction between a state with coexisting uniform SC and PDW order and a state with coexisting uniform SC and CDW order. First, the former state is expected to spontaneously break TRS. Second, we studied amplitude collective modes for PDW +SC and CDW +SC states and found that for a PDW+SC state, the spectral function of one collective mode displays a near- δ -function peak. We found that this mode is Raman active and argued that a sharp peak should be visible in the Raman intensity. There is no such sharp peak in a CDW +SC state, i.e., the peak is apparently a unique feature of the PDW+SC order. A peak in the symmetric A Raman channel at $\omega \sim 50 \text{cm}^{-1}$ has been reported in underdoped LSCO at $x \approx 0.1$ ⁵⁷. It is tempting to associate this peak with low-energy peak in the PDW +SC state, Fig. 3(b). However, since establishing this channel requires careful subtraction across multiple raw datasets, more intensive and rigorous measurements are needed to conclusively identify whether this is the case.

Data availability

Sequence data that support the findings of this study have been deposited at <https://doi.org/10.5281/zenodo.15670839>.

Received: 29 April 2025; Accepted: 21 July 2025;

Published online: 01 August 2025

References

1. Agterberg, D. F. et al. The physics of pair-density waves: Cuprate superconductors and beyond. *Annu. Rev. Condens. Matter Phys.* **11**, 231–270 (2020).
2. Wu, Y.-M., Wu, Z. & Yao, H. Pair-density-wave and chiral superconductivity in twisted bilayer transition metal dichalcogenides. *Phys. Rev. Lett.* **130**, 126001 (2023).
3. Wu, Y.-M., Nosov, P. A., Patel, A. A. & Raghu, S. Pair density wave order from electron repulsion. *Phys. Rev. Lett.* **130**, 026001 (2023).
4. Castro, P., Shaffer, D., Wu, Y.-M. & Santos, L. H. Emergence of the chern supermetal and pair-density wave through higher-order van hove singularities in the haldane-hubbard model. *Phys. Rev. Lett.* **131**, 026601 (2023).
5. Setty, C., Fanfarillo, L. & Hirschfeld, P. J. Mechanism for fluctuating pair density wave. *Nat. Commun.* **14**, 3181 (2023).

6. Jiang, H.-C. Pair density wave in the doped three-band hubbard model on two-leg square cylinders. *Phys. Rev. B* **107**, 214504 (2023).
7. Ticea, N. S., Raghu, S. & Wu, Y.-M. Pair density wave order in multiband systems. *Phys. Rev. B* **110**, 094515 (2024).
8. Jiang, Y.-F. & Yao, H. Pair-density-wave superconductivity: A microscopic model on the 2d honeycomb lattice. *Phys. Rev. Lett.* **133**, 176501 (2024).
9. Han, Z., Kivelson, S. A. & Yao, H. Strong coupling limit of the holstein-hubbard model. *Phys. Rev. Lett.* **125**, 167001 (2020).
10. Huang, K. S., Han, Z., Kivelson, S. A. & Yao, H. Pair-density-wave in the strong coupling limit of the holstein-hubbard model. *npj Quantum Mater.* **7**, 17 (2022).
11. Liu, F. & Han, Z. Pair density wave and $s \pm id$ superconductivity in a strongly coupled lightly doped kondo insulator. *Phys. Rev. B* **109**, L121101 (2024).
12. Wang, J. et al. Pair density waves in the strong-coupling two-dimensional holstein-hubbard model: a variational monte carlo study (2024). arXiv: 2404.11950.
13. Santos, L. H., Wang, Y. & Fradkin, E. Pair-density-wave order and paired fractional quantum hall fluids. *Phys. Rev. X* **9**, 021047 (2019).
14. Dai, Z., Zhang, Y.-H., Senthil, T. & Lee, P. A. Pair-density waves, charge-density waves, and vortices in high- T_c cuprates. *Phys. Rev. B* **97**, 174511 (2018).
15. Wang, H.-X. & Huang, W. Quantum-geometry-facilitated pair density wave order: Density matrix renormalization group study (2024). arXiv: 2406.17187.
16. Han, Z. & Kivelson, S. A. Pair density wave and reentrant superconducting tendencies originating from valley polarization. *Phys. Rev. B* **105**, L100509 (2022).
17. Shaffer, D. & Santos, L. H. Triplet pair density wave superconductivity on the π -flux square lattice. *Phys. Rev. B* **108**, 035135 (2023).
18. Agterberg, D. F. & Tsunetsugu, H. Dislocations and vortices in pair-density-wave superconductors. *Nat. Phys.* **4**, 639–642 (2008).
19. Wu, Y.-M. & Wang, Y. d-wave charge-4e superconductivity from fluctuating pair density waves. *npj Quantum Mater.* **9**, 66 (2024).
20. Chen, H. et al. Roton pair density wave in a strong-coupling kagome superconductor. *Nature* **599**, 222–228 (2021).
21. Deng, H. et al. Chiral kagome superconductivity modulations with residual fermi arcs. *Nature* **632**, 775–781 (2024).
22. Wu, Y.-M., Thomale, R. & Raghu, S. Sublattice interference promotes pair density wave order in kagome metals. *Phys. Rev. B* **108**, L081117 (2023).
23. Schwemmer, T. et al. Sublattice modulated superconductivity in the kagome hubbard model. *Phys. Rev. B* **110**, 024501 (2024).
24. Yao, M., Wang, Y., Wang, D., Yin, J.-X. & Wang, Q.-H. Self-consistent theory of 2×2 pair density waves in kagome superconductors arXiv: 2408.03056. (2024).
25. Jin, J.-T., Jiang, K., Yao, H. & Zhou, Y. Interplay between pair density wave and a nested fermi surface. *Phys. Rev. Lett.* **129**, 167001 (2022).
26. Scammell, H. D., Ingham, J., Li, T. & Sushkov, O. P. Chiral excitonic order from twofold van hove singularities in kagome metals. *Nat. Commun.* **14**, 605 (2023).
27. Liu, X., Chong, Y. X., Sharma, R. & Davis, J. C. S. Discovery of a cooper-pair density wave state in a transition-metal dichalcogenide. *Science* **372**, 1447–1452 (2021).
28. Cao, L. et al. Directly visualizing nematic superconductivity driven by the pair density wave in nbse2. *Nat. Commun.* **15**, 7234 (2024).
29. Shaffer, D., Burnell, F. J. & Fernandes, R. M. Weak-coupling theory of pair density wave instabilities in transition metal dichalcogenides. *Phys. Rev. B* **107**, 224516 (2023).
30. Gu, Q. et al. Detection of a pair density wave state in ute2. *Nature* **618**, 921–927 (2023).
31. Aishwarya, A. et al. Magnetic-field-sensitive charge density waves in the superconductor ute2. *Nature* **618**, 928–933 (2023).
32. Aishwarya, A. et al. Melting of the charge density wave by generation of pairs of topological defects in ute2. *Nat. Phys.* **20**, 964–969 (2024).
33. Zhao, H. et al. Smectic pair-density-wave order in eurbe4as4. *Nature* **618**, 940–945 (2023).
34. Devarakonda, A. et al. Evidence of striped electronic phases in a structurally modulated superlattice. *Nature* **631**, 526–530 (2024).
35. Han, T. et al. Signatures of chiral superconductivity in rhombohedral graphene arXiv: 2408.15233. (2024).
36. Moodenbaugh, A. R., Xu, Y., Suenaga, M., Folkerts, T. J. & Shelton, R. N. Superconducting properties of $la_{2-x}ba_xcuo_4$. *Phys. Rev. B* **38**, 4596–4600 (1988).
37. Li, Q., Hücker, M., Gu, G. D., Tsvelik, A. M. & Tranquada, J. M. Two-dimensional superconducting fluctuations in stripe-ordered $la_{1.875}ba_{0.125}cuo_4$. *Phys. Rev. Lett.* **99**, 067001 (2007).
38. Berg, E. et al. Dynamical layer decoupling in a stripe-ordered high- T_c superconductor. *Phys. Rev. Lett.* **99**, 127003 (2007).
39. Berg, E., Fradkin, E., Kivelson, S. A. & Tranquada, J. M. Striped superconductors: how spin, charge and superconducting orders intertwine in the cuprates. *N. J. Phys.* **11**, 115004 (2009).
40. Wang, Y., Agterberg, D. F. & Chubukov, A. Interplay between pair- and charge-density-wave orders in underdoped cuprates. *Phys. Rev. B* **91**, 115103 (2015).
41. Wang, Y., Agterberg, D. F. & Chubukov, A. Coexistence of charge-density-wave and pair-density-wave orders in underdoped cuprates. *Phys. Rev. Lett.* **114**, 197001 (2015).
42. Lee, P. A. Amperean pairing and the pseudogap phase of cuprate superconductors. *Phys. Rev. X* **4**, 031017 (2014).
43. Fradkin, E., Kivelson, S. A. & Tranquada, J. M. Colloquium: Theory of intertwined orders in high temperature superconductors. *Rev. Mod. Phys.* **87**, 457–482 (2015).
44. Huang, H. et al. Two-dimensional superconducting fluctuations associated with charge-density-wave stripes in $la_{1.87}sr_{0.13}cu_{0.99}fe_{0.01}o_4$. *Phys. Rev. Lett.* **126**, 167001 (2021).
45. Zhong, R. et al. Evidence for magnetic-field-induced decoupling of superconducting bilayers in $la_{2-x}ca_{1+x}cu_2o_6$. *Phys. Rev. B* **97**, 134520 (2018).
46. Shi, Z., Baity, P. G., Terzic, J., Sasagawa, T. & Popović, D. Pair density wave at high magnetic fields in cuprates with charge and spin orders. *Nat. Commun.* **11**, 3323 (2020).
47. Ding, J. F., Xiang, X. Q., Zhang, Y. Q., Liu, H. & Li, X. G. Two-dimensional superconductivity in stripe-ordered $la_{1.6-x}nd_{0.4}sr_xcuo_4$ single crystals. *Phys. Rev. B* **77**, 214524 (2008).
48. Hayden, S. M. & Tranquada, J. M. Charge correlations in cuprate superconductors. *Annu. Rev. Condens. Matter Phys.* **15**, 215–235 (2024).
49. Edkins, S. D. et al. Magnetic field-induced pair density wave state in the cuprate vortex halo. *Science* **364**, 976–980 (2019).
50. Du, Z. et al. Imaging the energy gap modulations of the cuprate pair-density-wave state. *Nature* **580**, 65–70 (2020).
51. Hamidian, M. H. et al. Detection of a cooper-pair density wave in $bi_2sr_2cacu_2o_{8+x}$. *Nature* **532**, 343–347 (2016).
52. Gao, Z.-Q., Lin, Y.-P. & Lee, D.-H. Pair-breaking scattering interference as a mechanism for superconducting gap modulation arXiv: 2310.06024. (2023).
53. Lee, J.-S. et al. Pair-density wave signature observed by x-ray scattering in la-based high- t_c cuprates arXiv: 2310.19907. (2023).
54. Soto-Garrido, R., Wang, Y., Fradkin, E. & Cooper, S. L. Higgs modes in the pair density wave superconducting state. *Phys. Rev. B* **95**, 214502 (2017).
55. Jian, S.-K., Scherer, M. M. & Yao, H. Mass hierarchy in collective modes of pair-density-wave superconductors. *Phys. Rev. Res.* **2**, 013034 (2020).
56. Nagashima, R., Moulleron, T. & Tsuji, N. Optically active higgs and leggett modes in multiband pair-density-wave superconductors with lifshitz invariant arXiv: 2410.18438. (2024).

57. Sugai, S. et al. Superconducting pairing and the pseudogap in the nematic dynamical stripe phase of $\text{La}_{2-x}\text{Sr}_x\text{CuO}_4$. *J. Phys.: Condens. Matter* **25**, 475701 (2013).
58. Loret, B. et al. Intimate link between charge density wave, pseudogap and superconducting energy scales in cuprates. *Nat. Phys.* **15**, 771–775 (2019).
59. Benhabib, S. et al. Three energy scales in the superconducting state of hole-doped cuprates detected by electronic raman scattering. *Phys. Rev. B* **92**, 134502 (2015).
60. Sugai, S., Takayanagi, Y. & Hayamizu, N. Phason and amplitudon in the charge-density-wave phase of one-dimensional charge stripes in $\text{La}_{2-x}\text{Sr}_x\text{CuO}_4$. *Phys. Rev. Lett.* **96**, 137003 (2006).
61. Tassini, L. et al. Dynamical properties of charged stripes in $\text{La}_{2-x}\text{Sr}_x\text{CuO}_4$. *Phys. Rev. Lett.* **95**, 117002 (2005).
62. Venturini, F. et al. Raman scattering versus infrared conductivity: Evidence for one-dimensional conduction in $\text{La}_{2-x}\text{Sr}_x\text{CuO}_4$. *Phys. Rev. B* **66**, 060502 (2002).
63. Lampakis, D., Liarokapis, E. & Panagopoulos, C. Micro-raman evidence for topological charge order across the superconducting dome of $\text{La}_{2-x}\text{Sr}_x\text{CuO}_4$. *Phys. Rev. B* **73**, 174518 (2006).
64. Hackl, R. et al. Raman study of ordering phenomena in copper-oxygen systems. *J. Phys. Chem. Solids* **67**, 289–293 (2006). Spectroscopies in Novel Superconductors 2004.
65. Muschler, B. et al. Electron interactions and charge ordering in CuO_2 compounds. *Eur. Phys. J. Spec. Top.* **188**, 131–152 (2010).
66. Gozar, A., Koomiya, S., Ando, Y. & Blumberg, G. *Magnetic and Charge Correlations in $\text{La}_{2-x-y}\text{Nd}_y\text{Sr}_x\text{CuO}_3$: Raman Scattering Study*, 755–789 (Springer Berlin Heidelberg, Berlin, Heidelberg, 2005).
67. Opel, M. et al. Carrier relaxation, pseudogap, and superconducting gap in high- T_c cuprates: A raman scattering study. *Phys. Rev. B* **61**, 9752–9774 (2000).
68. Miao, H. et al. Charge density waves in cuprate superconductors beyond the critical doping. *npj Quantum Mater.* **6**, 31 (2021).
69. Wen, J.-J. et al. Observation of two types of charge-density-wave orders in superconducting $\text{La}_{2-x}\text{Sr}_x\text{CuO}_4$. *Nat. Commun.* **10**, 3269 (2019).
70. Miao, H. et al. Formation of incommensurate charge density waves in cuprates. *Phys. Rev. X* **9**, 031042 (2019).
71. Lin, J. Q. et al. Strongly correlated charge density wave in $\text{La}_{2-x}\text{Sr}_x\text{CuO}_4$ evidenced by doping-dependent phonon anomaly. *Phys. Rev. Lett.* **124**, 207005 (2020).
72. Miao, H. et al. High-temperature charge density wave correlations in $\text{La}_{1.875}\text{Ba}_{0.125}\text{CuO}_4$ without spin-charge locking. *Proc. Natl Acad. Sci.* **114**, 12430–12435 (2017).
73. Peng, Y. Y. et al. Enhanced electron-phonon coupling for charge-density-wave formation in $\text{La}_{1.8-x}\text{Eu}_{0.2}\text{Sr}_x\text{CuO}_{4+\delta}$. *Phys. Rev. Lett.* **125**, 097002 (2020).
74. Benfatto, L., Toschi, A. & Caprara, S. Low-energy phase-only action in a superconductor: A comparison with the XY model. *Phys. Rev. B* **69**, 184510 (2004).
75. Paramekanti, A., Randeria, M., Ramakrishnan, T. V. & Mandal, S. S. Effective actions and phase fluctuations in d-wave superconductors. *Phys. Rev. B* **62**, 6786–6799 (2000).
76. Benfatto, L., Caprara, S., Castellani, C., Paramekanti, A. & Randeria, M. Phase fluctuations, dissipation, and superfluid stiffness in d-wave superconductors. *Phys. Rev. B* **63**, 174513 (2001).
77. See the supplementary information for i) details of the bogoliubov quasiparticle band structure, ii) mean-field gap equation and the identification of trsb , iii) details about obtaining the fluctuating part s_{FL} , including calculation of $\bar{\pi}$. iv) derivation of the raman susceptibility. (2025).
78. Baruch, S. & Orgad, D. Spectral signatures of modulated d-wave superconducting phases. *Phys. Rev. B* **77**, 174502 (2008).
79. Norman, M. R. & Davis, J. C. S. Quantum oscillations in a biaxial pair density wave state. *Proc. Natl Acad. Sci.* **115**, 5389–5391 (2018).
80. Zelli, M., Kallin, C. & Berlinsky, A. J. Quantum oscillations in a π -striped superconductor. *Phys. Rev. B* **86**, 104507 (2012).
81. Caplan, Y. & Orgad, D. Quantum oscillations from a pair-density wave. *Phys. Rev. Res.* **3**, 023199 (2021).
82. Karapetyan, H. et al. Evidence of chiral order in the charge-ordered phase of superconducting $\text{La}_{1.875}\text{Ba}_{0.125}\text{CuO}_4$ single crystals using polar kerr-effect measurements. *Phys. Rev. Lett.* **112**, 047003 (2014).
83. Li, L., Alidoust, N., Tranquada, J. M., Gu, G. D. & Ong, N. P. Unusual nernst effect suggesting time-reversal violation in the striped cuprate superconductor $\text{La}_{2-x}\text{Ba}_x\text{CuO}_4$. *Phys. Rev. Lett.* **107**, 277001 (2011).
84. Marciani, M., Fanfarillo, L., Castellani, C. & Benfatto, L. Leggett modes in iron-based superconductors as a probe of time-reversal symmetry breaking. *Phys. Rev. B* **88**, 214508 (2013).
85. Maiti, S. & Chubukov, A. V. $s + is$ state with broken time-reversal symmetry in fe-based superconductors. *Phys. Rev. B* **87**, 144511 (2013).
86. Phan, D. & Chubukov, A. V. Following the higgs mode across the bcs-bec crossover in two dimensions. *Phys. Rev. B* **107**, 134519 (2023).
87. Lin, S.-Z. & Hu, X. Massless leggett mode in three-band superconductors with time-reversal-symmetry breaking. *Phys. Rev. Lett.* **108**, 177005 (2012).
88. Burnell, F. J., Hu, J., Parish, M. M. & Bernevig, B. A. Leggett mode in a strong-coupling model of iron arsenide superconductors. *Phys. Rev. B* **82**, 144506 (2010).
89. Sharapov, S. G., Gusynin, V. P. & Beck, H. Effective action approach to the leggett's mode in two-band superconductors. *Eur. Phys. J. B - Condens. Matter Complex Syst.* **30**, 45–51 (2002).
90. Nosov, P. A., Andriyakhina, E. S. & Burmistrov, I. S. Spatially-resolved dynamics of the amplitude schmid-higgs mode in disordered superconductors arXiv: 2409.11647. (2024).
91. Lee, C. & Chung, S. B. Linear optical response from the odd-parity bardasis-schrieffer mode in locally non-centrosymmetric superconductors. *Commun. Phys.* **6**, 307 (2023).
92. Schött, J. et al. Analytic continuation by averaging padé approximants. *Phys. Rev. B* **93**, 075104 (2016).
93. Morr, D. K. & Pines, D. The resonance peak in cuprate superconductors. *Phys. Rev. Lett.* **81**, 1086–1089 (1998).
94. Fradkin, E. *Quantum field theory: an integrated approach* (Princeton University Press, 2021).
95. Browne, D. A. & Levin, K. Collective modes in charge-density-wave superconductors. *Phys. Rev. B* **28**, 4029–4032 (1983).
96. Torchinsky, D. H., Mahmood, F., Bollinger, A. T., Božović, I. & Gedik, N. Fluctuating charge-density waves in a cuprate superconductor. *Nat. Mater.* **12**, 387–391 (2013).
97. Lee, P. A., Rice, T. M. & Anderson, P. W. Fluctuation effects at a peierls transition. *Phys. Rev. Lett.* **31**, 462–465 (1973).
98. Littlewood, P. B. & Varma, C. M. Amplitude collective modes in superconductors and their coupling to charge-density waves. *Phys. Rev. B* **26**, 4883–4893 (1982).
99. Grüner, G. The dynamics of charge-density waves. *Rev. Mod. Phys.* **60**, 1129–1181 (1988).
100. Cea, T. & Benfatto, L. Nature and raman signatures of the higgs amplitude mode in the coexisting superconducting and charge-density-wave state. *Phys. Rev. B* **90**, 224515 (2014).
101. Grasset, R. et al. Higgs-mode radiance and charge-density-wave order in $2h - \text{nbse}_2$. *Phys. Rev. B* **97**, 094502 (2018).
102. Cea, T. & Benfatto, L. Signature of the leggett mode in the A_{1g} raman response: From MgB_2 to iron-based superconductors. *Phys. Rev. B* **94**, 064512 (2016).
103. Klein, M. V. & Dierker, S. B. Theory of raman scattering in superconductors. *Phys. Rev. B* **29**, 4976–4991 (1984).

104. Klein, M. V. Theory of raman scattering from leggett's collective mode in a multiband superconductor: Application to MgB_2 . *Phys. Rev. B* **82**, 014507 (2010).
105. Devereaux, T. P. & Hackl, R. Inelastic light scattering from correlated electrons. *Rev. Mod. Phys.* **79**, 175–233 (2007).
106. Chubukov, A. V. & Frenkel, D. M. Resonant two-magnon raman scattering in parent compounds of high- T_c superconductors. *Phys. Rev. B* **52**, 9760–9783 (1995).
107. Devereaux, T. P. & Einzel, D. Electronic raman scattering in superconductors as a probe of anisotropic electron pairing. *Phys. Rev. B* **51**, 16336–16357 (1995).
108. Devereaux, T. P. et al. Electronic raman scattering in high- T_c superconductors: A probe of $d_x^2-y^2$ pairing. *Phys. Rev. Lett.* **72**, 396–399 (1994).
109. Mross, D. F. & Senthil, T. Stripe melting and quantum criticality in correlated metals. *Phys. Rev. B* **86**, 115138 (2012).
110. Mross, D. F. & Senthil, T. Spin- and pair-density-wave glasses. *Phys. Rev. X* **5**, 031008 (2015).
111. Zyuzin, A. & Spivak, B. Theory of $\pi/2$ superconducting josephson junctions. *Phys. Rev. B* **61**, 5902–5904 (2000).
112. Yuan, A. C., Vituri, Y., Berg, E., Spivak, B. & Kivelson, S. A. Inhomogeneity-induced time-reversal symmetry breaking in cuprate twist junctions. *Phys. Rev. B* **108**, L100505 (2023).
113. Hirota, K. Neutron scattering studies of zn-doped $\text{La}_{2-x}\text{Sr}_x\text{CuO}_4$. *Phys. C: Superconductivity* **357–360**, 61–68 (2001).
114. Suchaneck, A. et al. Incommensurate magnetic order and dynamics induced by spinless impurities in $\text{YBa}_2\text{Cu}_3\text{O}_{6.6}$. *Phys. Rev. Lett.* **105**, 037207 (2010).

Acknowledgements

We thank Eduardo Fradkin, Rudi Hackl, Tom Devereaux, Suk Bum Chung and Saurabh Maiti for helpful discussions. Y.-M.W. acknowledges support from the Gordon and Betty Moore Foundation's EPiQS Initiative through GBMF8686. S.A.K. was supported in part by the Department of Energy, Office of Basic Energy Sciences, under contract No. DEAC02-76SF00515. A.V.C. was supported by the NSF-DMR Grant No. 2325357. Y. Wang was supported by NSF-DMR Grant No. 2045781. Y. Wang and A.V.C. acknowledge support by grant NSF PHY-1748958 to the Kavli Institute for Theoretical Physics (YW and MY), where this work was partly performed.

Author contributions

All authors performed analytic calculations. Y. Wu performed the numerical calculations. All authors wrote and reviewed the manuscript.

Competing interests

The authors declare no competing interests.

Additional information

Supplementary information The online version contains supplementary material available at <https://doi.org/10.1038/s41535-025-00808-w>.

Correspondence and requests for materials should be addressed to Yi-Ming Wu.

Reprints and permissions information is available at <http://www.nature.com/reprints>

Publisher's note Springer Nature remains neutral with regard to jurisdictional claims in published maps and institutional affiliations.

Open Access This article is licensed under a Creative Commons Attribution-NonCommercial-NoDerivatives 4.0 International License, which permits any non-commercial use, sharing, distribution and reproduction in any medium or format, as long as you give appropriate credit to the original author(s) and the source, provide a link to the Creative Commons licence, and indicate if you modified the licensed material. You do not have permission under this licence to share adapted material derived from this article or parts of it. The images or other third party material in this article are included in the article's Creative Commons licence, unless indicated otherwise in a credit line to the material. If material is not included in the article's Creative Commons licence and your intended use is not permitted by statutory regulation or exceeds the permitted use, you will need to obtain permission directly from the copyright holder. To view a copy of this licence, visit <http://creativecommons.org/licenses/by-nc-nd/4.0/>.

© The Author(s) 2025